Lignocellulosic agro-residue/polylactic acid (PLA) biocomposites: Rapeseed straw as a sustainable filler

László Lendvai

Department of Materials Science and Engineering, Széchenyi István University, H-9026, Győr, Egyetem tér 1., Hungary

ARTICLE INFO

ABSTRACT

The main objective of this study is to review the applicability of rapeseed straw (RSS) as a sustainable filler material in polylactic acid (PLA)-based biocomposites. The effect of different RSS particle sizes and concentrations (0–20 wt%) on the mechanical, morphological, thermal, and water absorption properties was investigated. The composites were fabricated by melt compounding using a twin-screw extruder followed by injection molding. The mechanical properties were analyzed through tensile and flexural tests and Charpy impact tests. The morphology of the samples was investigated by scanning electron microscopy (SEM). The thermal properties and the crystallinity of the composites were determined through differential scanning calorimetry (DSC). Mechanical properties revealed an increasing stiffness of PLA as a function of RSS loading, albeit at the cost of strength. SEM images have shown a limited interfacial adhesion between PLA and the straw, which was suggested to be responsible for the decreased strength values. Based on the DSC measurements, the RSS fibers facilitated the nucleation in the composites, thereby decreasing the cold crystallization temperature of PLA. The conducted experiments demonstrated that environmentally friendly and economically attractive biocomposites can be fabricated by substituting part of the PLA with RSS as a lignocellulosic by-product.

Introduction

In the past few decades gradually depleting fossil resources along with the pollution caused by drastically accumulating plastic waste have acted as an important driving force for the development of environmentally friendly polymeric materials. To reduce the contribution of plastics to worldwide generated waste, intensive research is being carried out. Currently, there are two major routes, when it comes to sustainable polymer development. Accordingly, there are i) studies promoting the reuse and recycling of traditional plastics (Ronkay et al., 2021; Lendvai et al., 2022), while other experiments are aimed at ii) the fabrication of novel, partly/entirely biodegradable polymeric materials.

In this latter respect, poly(lactic acid) (PLA) has received considerable attention as a "green" alternative. PLA is a linear aliphatic thermoplastic copolyester derived from renewable resources, and is also biodegradable at the same time. It has physical and mechanical properties similar to poly(ethylene terephthalate) (PET). Besides its obvious benefits, PLA also exhibits some disadvantages, therefore it is often paired with other materials to prepare polymer blends or composites with tailored properties. When it comes to technical applications the major drawbacks are its low heat resistance and toughness, while for commodity applications its rather high price. Even though PLA is considered a relatively inexpensive material within the group of biodegradable polymers, its average cost of ~5 €/kg is still several times higher than that of petrol-based commodity plastics, which greatly limits its potential to substitute petrochemical polymers like polypropylene (PP) or polystyrene (PS). In order to reduce the cost of plastics, while making them also environmentally friendlier, one of the most commonly used methods is to incorporate low-cost filler materials into them (Väisänen et al., 2016). Hence, considerable efforts have been devoted to the research and development of multicomponent polymeric systems containing agricultural and/or forest industry by-products in order to improve the matrix materials' performance, while also decreasing the overall production costs of the designed products (Lendvai et al., 2023; Singh et al., 2023b; Nweze Nwogu et al., 2022; Mishra et al., 2022). Following this principle, various natural resources have been employed to fabricate polymer composites, including hemp, bamboo, wheat straw, coconut shell, maize hull, sunflower husk, rice husk, etc. The straw leftover from harvested crops is one of the world's largest biomass resources (Amalina et al., 2022). According to estimations, straw makes up over 50% of the yield of crops (Wen et al., 2020). Unfortunately, in many countries, open-air burning is still a popular

method to get rid of unnecessary agricultural residues despite the fact that burning straws is an illegal activity (Yaashikaa et al., 2022). During this process, numerous harmful pollutants (CO, CO_2, CH_4, SO_2, NH_3, etc.) are released that are responsible for the deterioration of air quality and consequently affect public health (Yaashikaa et al., 2022; Bhattacharyya et al., 2021; Pang et al., 2022; Wang et al., 2020). Up to now, extensive studies have been performed on potential routes of crop straw valorization to promote sustainable waste management. These studies are mostly centered on the utilization of straws for energetic purposes or using them as additives in composite materials.

Rapeseed – which is traditionally used for animal feeding and vegetable oil production – is one of the most abundant crops worldwide with an annual production of 75 million metric tons (https://www.statista.com/statistics/263930/worldwide-production-of-rapeseed-by-country). Therefore, the proper handling of rapeseed straw (RSS) waste is a vital social concern, and it receives more and more interest in association with biodiesel production (Elsayed et al., 2022). The crop: straw ratio of rapeseed is rather high, roughly 2:3. Being a lignocellulosic agro-residue, RSS is composed of three major components; cellulose (33–50%), hemicellulose (12–25%) and lignin (17–29%) (Gaballah et al., 2020; Wang et al., 2020; Ji et al., 2014; Žiganova et al., 2022).

The development of natural (waste) fiber-filled polymer composites (NFRPCs) is a constantly growing field. Particularly within vehicle production, it is a proper strategy to utilize straw fiber-filled NFRPCs and resources. The main idea behind it is to create novel structural materials for various uses by combining polymeric materials with vegetable-based lignocellulosic by-products. The resulting composites potentially exhibit enhanced mechanical and physical properties relative to the parent polymer, and additionally, fewer petrochemicals will be required for the production, since part of the plastics can be replaced by "green" low-cost fillers that are considered as waste otherwise. This makes the fabricated composites more environmentally friendly and cheap. Due to the above-mentioned benefits, numerous recent studies have been aimed to find an effective purpose for the available crop straw resources (Bilal et al., 2017; Tian et al., 2018; Sohni et al., 2018; Zeleke et al., 2023; Pascoli et al., 2022). If the used polymer matrix is also a biopolymer (like PLA), then there is an additional advantage, namely that the fabricated composites will be entirely biodegradable as well (Zeleke et al., 2023; Ranakoti et al., 2022; Beniwal and Toor, 2023; Wang et al., 2022). Owing to their decent strength, excellent stiffness, and the fact that they can be processed with common manufacturing techniques, NFRPCs find extensive applications in various fields, such as the automotive, building, biomedical, and electronic industries (Väisänen et al., 2016; Wang et al., 2020; Singh, 2021; Ranakoti et al., 2022).

Zhang et al. (Zhang et al., 2020) fabricated wheat straw-reinforced, recycled polyethylene-based composites and analyzed the effect of wheat straw content (20–60 wt%) and fiber size on the properties. It was found that the tensile strength of the composites increased up until 50 wt% straw content; above that, however, it deteriorated. Meanwhile, both the tensile and flexural modulus increased gradually. On the other hand, the elongation at break of the polyethylene was gradually reduced. Regarding fiber length, long fibers were preferred for their higher strength and stiffness, while shorter fibers enabled more deformability. Feng et al. (Feng et al., 2020) tested four different kinds of straw fibers (sorghum, rice, corn, and soybean) as fillers in PLA/poly(butylene-adipate-*co*-terephthalate) blends. Superior mechanical properties were found for soybean straw-filled samples, which was attributed to their highest cellulose content. It was followed by rice straw, sorghum straw, and corn straw, respectively. The corn straw-filled composite, as the worst choice, exhibited 25.3% lower tensile strength, 14.6% lower flexural strength, and 27.8% lower impact strength than those blends filled with soybean. These major differences were explained by the loose structure of the corn straw's inner core, which was difficult to be soaked by the matrices. In the study of Qi et al. (Qi et al., 2022) the authors used corn straw fibers (30 wt%) as fillers in PLA-based biocomposites. The

fibers were classified according to their size in the ranges of 20–40 mesh, 40–80 mesh, 80–120 mesh, and >120 mesh. PLA showed to be superior regarding its tensile and bending strength against all composites. Among the PLA/corn straw composites the ones with the lowest particle size exhibited the best mechanical properties. Pongputthipat et al. (Pongputthipat et al., 2022) used rice straw as reinforcement in PLA/natural rubber films with 3–10 wt% straw powder. The presence of rice straw led to improved Young's modulus, although at the cost of tensile strength and elongation at break.

As outlined above, recent years have seen numerous studies being devoted to exploiting the potential of various agro-residues in polymer-based biocomposites, including the ones with PLA matrix. In this respect, RSS is an exception, since there are no reports in the literature about pairing this abundant vegetable by-product with PLA up to this point. In this research, RSS-filled composites have been prepared using PLA as matrix material to offer a potential substitute for commodity plastics in single-use applications. Both the size and the concentration of the straw particles were varied in order to understand their effect on the behavior of the polymer matrix. Mechanical, morphological, thermal, and physical properties have been analyzed to explore the structure–property relationships of the developed composite samples.

Materials and methods

Materials

The PLA used as the polymer matrix of the biocomposites was the Ingeo Biopolymer 2003D grade produced by NatureWorks Ltd. (Minnetonka, MN, USA). According to its datasheet, this polymer has a specific density of 1.24 g/cm^3, a D-isomer content of 4%, a melting temperature of 170 °C, and a melt flow rate of 6 g/10 min (at 210 °C and 2.16 kg).

Chopped RSS as lignocellulosic biomass with a fiber length of 30–50 mm was supplied by Mikó Stroh Borotai-Laska Ltd. (Baja, Hungary). The biomass was washed using purified water in order to eliminate potential contaminations and then dried in a heated oven. Subsequently, the dry straw fibers were ground using a feed grinder and then sieved with a Matest A059 sieve shaker (Treviolo, Italy). The particles were fractioned through sieving into three groups according to their size: large, medium, and small. The large fraction (L) was collected from the sieves between 35 and 60 mesh (500–250 μm), the medium (M) from the sieves between 60 and 120 mesh (250–125 μm), while the small (S) fraction from the sieves between 120 and 250 mesh (125–63 μm).

Preparation and processing

Before the melt compounding, both the RSS fibers and the polymer granules were dried in a Faithful WGLL-125BE type air-circulating dehumidifier (Huanghua, Cangzhou, China) at 80 °C for 4 h to prevent the hydrolytic degradation of PLA throughout the processing. Subsequently, composites with varying RSS concentrations and particle sizes were prepared through melt mixing. The melt compounding was carried out using a Labtech twin-screw extruder model LTE 20–44 (Samut Prakarn, Thailand) with a screw diameter of 20 mm and a length-to-diameter ratio of 44. The temperatures of heating zones along the extruder barrel were set to 155–185 °C from feeder to die, while the rotational speed of the screws was 30 rpm. The extruded strings were solidified using an immersion cooling tank filled with distilled water. After that, granules were obtained by pelletizing the solid composite strings with a Labtech LZ-120/VS type strand pelletizer (Samut Prakarn, Thailand). The formulations of the fabricated biocomposites are shown in Table 1.

In order to achieve sample geometries suitable for characterization, injection molding was applied as the next step of preparation. For this purpose, an Arburg Allrounder Advance 420C injection molding machine (Lossburg, Germany) was used, which was equipped with a 35 mm

Table 1
List of materials prepared in this work with their designations and composition.

Designation	PLA content [wt %]	Rapeseed straw content [wt%]	Rapeseed straw size
PLA	100	0	–
PLA_2.5_M	97.5	2.5	M (60–120 mesh)
PLA_5_M	95	5	M (60–120 mesh)
PLA_10_M	90	10	M (60–120 mesh)
PLA_20_M	80	20	M (60–120 mesh)
PLA_10_S	90	10	S (120–250 mesh)
PLA_10_L	90	10	L (35–60 mesh)

screw. Note that before the injection molding, both PLA and the PLA-based biocomposite granules were dried once more under the same conditions as they were dried prior to the extrusion, to remove their inherent moisture content. During the injection molding a mold with a twin cavity of dogbone-shaped specimens (EN ISO 527-2, type A) was equipped onto the machine. Injection molding was performed at a barrel temperature ranging from 175 to 195 °C, while the mold temperature was fixed at 30 °C. The injection speed was 40 cm^3/s, and the holding pressure lasted for 15 secs with a pressure profile of 750–650-250 bar. For tensile tests, the injection molded specimens were used directly, while for the flexural tests and Charpy impact tests the ends (gripping parts) of the specimens were removed through cutting to obtain rectangular bars.

Characterization

Particle size analysis

Particle size analysis of the RSS fibers was performed based on optical microscopic images acquired by a Zeiss Axio Imager A1 stereomicroscope (Carl Zeiss, Oberkochen, Germany). RSS fibers were well spread on a homogenous black plastic platform in a way that they would not overlap each other. To determine the particle size of the L, M, and S fractions, the fiber width and length of at least 1000 particles in each fraction were measured manually using the integrated numerical caliper of the applied optical microscopes' dedicated software. Based on the results the mean length, width, and aspect ratio of each fraction were calculated.

Differential scanning calorimetry

Differential scanning calorimetric (DSC) measurements were performed by a Netzsch DSC 200 F3 calorimeter (Selb, Germany). Samples of ~5 mg were analyzed under nitrogen flow. Firstly, the specimens were heated up from 25 °C to 200 °C and maintained at 200 °C for 5 mins. Subsequently, the samples were cooled down to 25 °C at 5 °C/min and then heated up once more to 200 °C at a rate of 5 °C/min. The thermal properties were determined based on the second heating, while the first heating run served the purpose of erasing the thermal history of the samples. The crystallinity degree was determined using Equation (1):

$$x_c = \frac{\Delta H_m}{\Delta H_m^\infty \times \omega_{PLA}} \tag{1}$$

where X_c is the degree of crystallinity of PLA, ΔH_m (J/g) is the heat of fusion of PLA, ΔH_m^∞ (J/g) is the heat of fusion of 100% crystalline PLA (taken as 93.7 J/g (Zhang et al., 2020) and ω_{PLA} is the weight fraction of PLA in the sample.

Scanning electron microscopy

The morphology of the fracture surfaces obtained through the impact tests was observed by scanning electron microscopy (SEM) at an acceleration voltage of 10 kV using a Hitachi S-3400 N apparatus (Tokyo, Japan). The samples were sputter coated with a gold layer before SEM inspection to prevent charging. For this purpose, a Quorum SC7620 sputter-coater (Lewes, UK) was used.

Mechanical properties

The tensile tests were conducted according to the EN ISO 527 standard by using a double-column universal testing machine model Instron 5582 (Norwood, Massachusetts, USA) equipped with a load cell of 10 kN. The initial gauge length was 100 mm, and the strain rate was 5 mm/min. The flexural tests were carried out in accordance with the EN ISO 178 on the same Instron 5582 machine that was used for the tensile tests. Flexural tests were performed using rectangular specimens of 80 × 4 × 10 mm, and a span length of 64 mm. Impact testing was performed according to the EN ISO 179 standard using a Ceast 6545 pendulum machine (Pianezza, Italy) in Charpy-mode. An impact energy of 2 J was applied on un-notched samples. The specimens used for this measurement were rectangular bars of 80 × 4 × 10 mm with a bearing distance of 62 mm. The tensile, flexural, and impact tests were repeated five times for all samples in order to ensure reproducibility. Average values and standard deviations were calculated from these five repetitive measurements. All data were statistically elaborated by analysis of variance (ANOVA) and compared using Tukey's test at a 5% significance level.

Dynamic mechanical analysis

The dynamic mechanical analysis (DMA) of the PLA/RSS composites was performed by using a TA DMA Q800 instrument (New Castle, Delaware, USA). The specimens were analyzed with a dual cantilever grip at 1 Hz from 25 °C to 150 °C with a heating rate of 2 °C/min. The storage modulus and loss factor were determined as a function of temperature for all of the specimens with an amplitude of 20 μm.

Water absorption

In order to study the water absorption, three specimens of each sample were immersed in deionized water at room temperature. Prior to the immersion, all the samples were dried until a constant weight was achieved. The samples were taken out periodically to record the gain in weight. After being removed from the distilled water, the surface of the samples was wiped using a paper towel to remove any excess moisture. The percentage of water absorption was calculated by Equation (2):

$$Water\ absorbed(\%) = \frac{W_t - W_0}{W_0} \times 100 \tag{2}$$

where W_t is the weight of the sample at time t after exposure to water, while W_0 is the initial dry weight.

Results and discussion

RSS fiber size measurements

Fig. 1 shows optical microscopic images (Fig. 1a, c, e), and the fiber length /fiber width distributions of the three RSS factions (Fig. 1b, d, f), while Table 2 represents the calculated mean values, standard deviations and aspect ratios. The width distribution of S-, M- and L-sized straw fibers exceeding 90% was found to be in the range of 45–125 μm (Fig. 1b), 75–230 μm (Fig. 1d), and 130–430 μm (Fig. 1f), with mean values of 79 μm, 137 μm, and 254 μm, respectively. Meanwhile, the length distribution of the three factions concentrated in the range of 100–390 μm, 200–690 μm, and 470–1700 μm, respectively. Apparently, the mean length of L–sized fibers was considerably larger relative to its width, when compared to the M and S fractions, resulting in the highest aspect ratio of 3.79. On the other hand, the S-sized fibers had the lowest aspect ratio, indicating that these particles had the least "fiber-like" geometry out of the three.
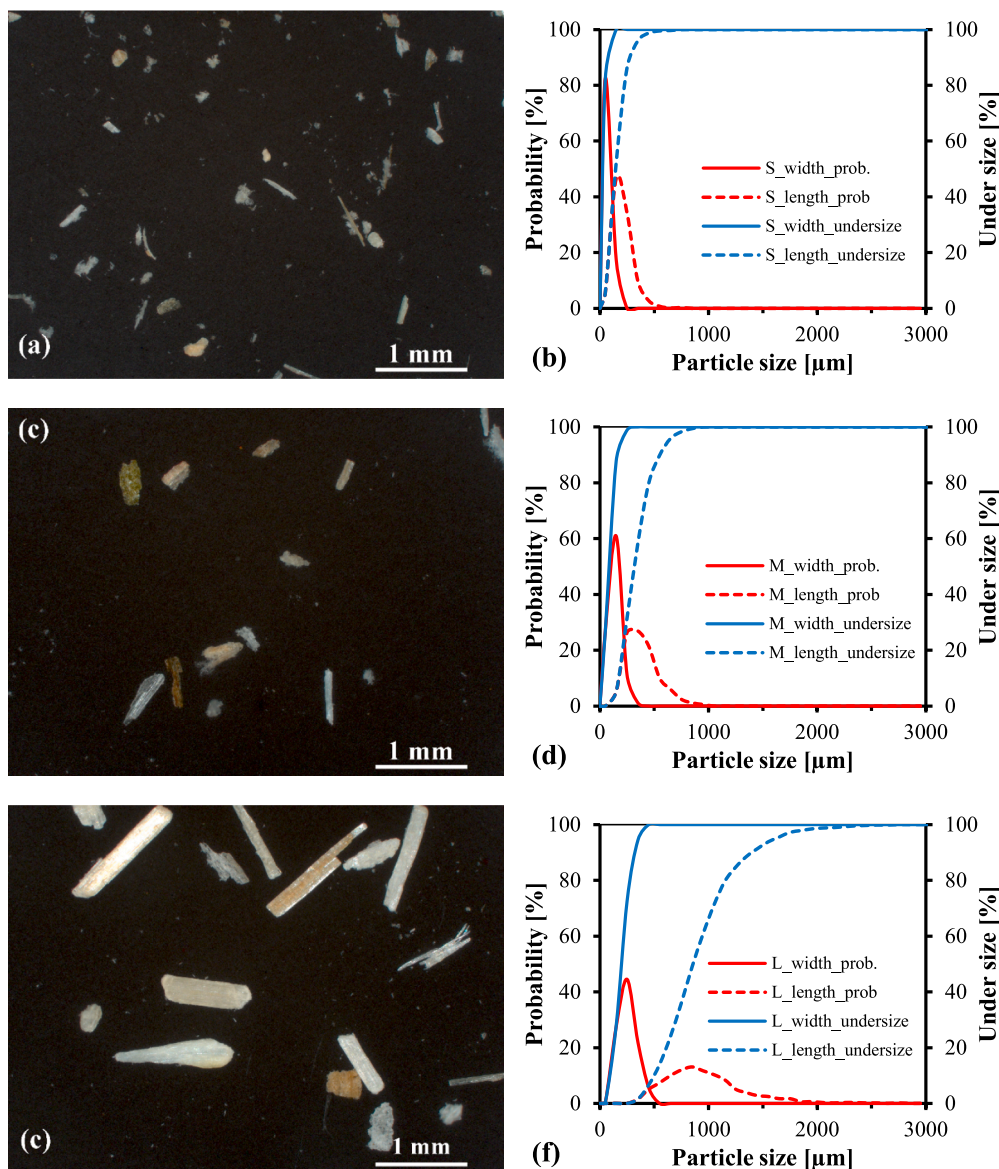
Fig. 1. Microscopic images and width/length distribution of RSS particles of various sizes – S: 120–250 mesh (a, b); M: 60–120 mesh (c, d); L: 35–60 mesh (e, f).

Table 2
The mean values of RSS length and width for the various size fractions (S, M, L) and their aspect ratio.

Straw fraction	Mesh size	Length [μm]	Width [μm]	Aspect ratio [-]
S	120–250	212 ± 91	79 ± 24	2.68
M	60–120	391 ± 150	137 ± 53	2.85
L	35–60	963 ± 366	254 ± 81	3.79

Differential scanning calorimetry

Fig. 2 depicts the DSC thermograms recorded during the second heating run of unfilled PLA and the PLA/RSS composites, while Table 3 shows the thermal properties obtained from the curves, such as glass transition temperature, cold crystallization temperature, melting temperature, cold crystallization enthalpy, melting enthalpy, and crystallinity ratio. The unfilled PLA sample showed three thermal transitions. The first one was a shift in the baseline at 60.2 °C, indicating the glass transition (T_g). The T_g was followed by the cold crystallization (T_{cc}) in a form of an exothermic peak, exhibiting its maximum at 105.7 °C. Even though PLA is a semi–crystalline polymer, due to its relatively slow
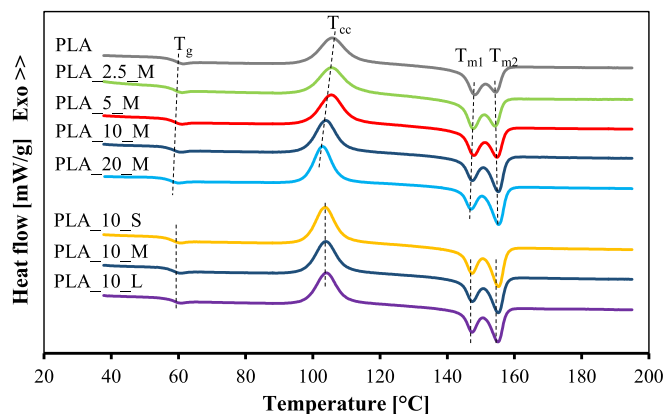

Fig. 2. Characteristic DSC curves of the fabricated samples (second heating run).

Table 3
Data obtained from the DSC analyses.

Sample	T_g [°C]	T_{cc} [°C]	ΔH_{cc} [J/g]	T_{m1} [°C]	T_{m2} [°C]	ΔH_m [J/g]	X_c [%]
PLA	60.2	105.7	24.8	148.3	154.4	24.9	26.5
PLA_2.5_M	59.1	105.5	26.1	147.8	154.4	26.2	28.7
PLA_5_M	58.8	105.4	25.9	147.8	154.7	26.2	29.4
PLA_10_M	58.5	103.7	25.8	147.4	155.2	26.7	31.6
PLA_20_M	58.3	102.9	25.1	147.3	155.3	25.9	34.6
PLA_10_S	58.7	103.7	27.3	147.3	155.3	28.2	33.4
PLA_10_L	58.7	103.9	23.9	147.4	155.2	24.8	29.4

crystallization kinetics it remained in a rather amorphous structure throughout its cooling from the melt. Therefore, in the temperature range of 90–125 °C the increased chain mobility facilitated the arrangement of PLA molecules into crystalline phases. The last transition observed on the DSC curve of PLA was related to the melting of the crystalline domains, which occurred as an endothermic double peak in the temperature range of 125–160 °C. The temperature corresponding to the first, slightly larger melting peak (T_{m1}) was at 148.3 °C, while the second one (T_{m2}) was at 154.4 °C For the double melting of PLA, multiple theories can be found within the literature (Yasuniwa et al., 2004; Ambrosio-Martín et al., 2014). Yasuniwa et al. (Yasuniwa et al., 2004) attributed this double melting phenomenon to a melt-recrystallization process. According to the suggested model, the melt-recrystallization enables the small and imperfect crystals to transform successively into more stable crystals. Following this theory, there are two crystalline species present in PLA (α and β), one of which is less ordered, than the other. Considering that recrystallization is a time-consuming process, the amount of the recrystallized crystals is limited and it depends on a number of factors. There is also another hypothesis, according to which there is only a single crystalline species that comes with two different crystalline morphologies (Tábi et al., 2016; Zhang et al., 2008). The main difference between these two variations is that the one denoted as α is more stable, thereby it exhibits a higher melting temperature compared to the less stable α' metaphase. The amount of α and α' polymorphs is dependent on the temperature where the crystallization took place. When the crystallites are formed below 100 °C, then the less ordered α'gets developed, while above 120 °C the stable α is the preferred polymorph. If the crystallization occurs between these two temperatures (100 and 120 °C) then a combination of the two polymorphs will be formed, which ultimately leads to the double melting behavior. The melting enthalpy (ΔH_m: 24.9 J/g) calculated through the integration of the double peaks roughly equals the enthalpy value that was determined for the cold crystallization (ΔH_{cc}: 24.8 J/g). This supports the assumption made previously, namely that the PLA was rather amorphous before the heating run.

The incorporation of RSS in various concentrations into PLA altered the characteristic transition temperatures of PLA, as is also indicated in Fig. 2 with the dashed lines. The T_g shifted to slightly lower temperatures in the presence of RSS. Even though rigid filler particles tend to increase the T_g, the glass transition temperature of polymer composites depends on numerous factors, one of which is the characteristics of the interphase between the components. A reduction in T_g generally indicates a poor interfacial adhesion between the matrix and the reinforcement. (Tao et al., 2017; Lee et al., 2008). The temperature of cold crystallization gradually decreased with growing RSS concentration, bottoming at 102.9 °C for the PLA_20_M sample. This earlier crystallization during heating can be ascribed to the nucleating effect of RSS particles on the polymer, an assumption which is also supported by the fact that not only the crystallization started earlier, but the ratio of crystallinity also increased from 26.5% up to 34.6%. At the same time, the ratio of the two melting peaks also altered, with the second one becoming more dominant with increasing RSS. In the case of the α' and α theory, the opposite was to be expected considering the reduced T_{cc} values. Accordingly, the melt-recrystallization mechanism is more justified in this case, which

was greatly facilitated by the presence of RSS particles based on the current results. The characteristic temperatures of the crystalline melting were barely affected by the presence of RSS. The melting peaks of the two crystalline species were recorded in the small range of 147.8 ± 0.5 °C and 154.9 ± 0.5 °C, respectively, for all composite samples.

There was barely any change in the characteristic transition temperatures, regardless of the straw's sizes; however, the smaller particles resulted in a considerably higher crystallinity ratio, which is suggested to be due to the larger number of particles (more nucleation sites), when they are incorporated in the same weight ratio.

SEM analysis

In order to understand and justify the mechanical behavior of the fabricated samples, SEM analysis was performed. The micrographs of the fracture surfaces obtained after the impact tests are shown in Fig. 3. As seen in Fig. 3a the fracture surface of the unfilled PLA is rather smooth, barely any pores or voids can be seen, similar to that already presented in the literature (Tao et al., 2017). On the other hand, with the addition of RSS, the surface becomes rather rough, while voids and micro-cracks get formed. Even though the straw particles seem well encapsulated within the PLA matrix regardless of the fiber size (Fig. 3b, c,d), gaps can be observed between them, indicating poor wettability, and as a result barely any adhesion between the components. This assumption seems rather reasonable, considering the fact that PLA has a non-polar surface making it hydrophobic, while straw, with its polar surface is rather hydrophilic. This and the cellular structure of the RSS particles can both be a source of the deteriorating mechanical properties of the PLA/straw composites (Mengeloglu and Karakus, 2008), as seen later. Meanwhile, the straw particles tend to have a rather rough surface, which is assumed to enable some stress transfer through mechanical interlocking between the polymer matrix and the filler particles, especially for the ones with a higher aspect ratio.

Tensile and flexural mechanical properties

The results of the quasi-static tensile and flexural mechanical properties are summarized in Table 4, whereas the representative stress-strain curves recorded during the tensile and flexural tests are plotted in Fig. 4.

Generally, composites with increasing RSS content exhibited slightly lower tensile strength values than neat PLA because of the lack of interfacial load-transfer capacity between the hydrophobic polymer matrix and the hydrophilic straw particles. As a consequence, the initial tensile strength of PLA (57.3 MPa) dropped by ~10 MPa, when 20 wt% of RSS was added to it. During the last several years, a large body of work has been devoted to overcoming this drop in strength of NFRPCs by the introduction of additional chemicals as coupling agents or using surface treatment on the fibers, thereby improving interfacial adhesion (Lendvai and Patnaik, 2022). However, taking this route greatly reduces the "green" characteristics of the fabricated composites, making them less environmentally friendly. Besides, the resulting strength values of all the composites prepared in this study are still considerably higher than of those petrochemical polymeric materials that are currently being used for single-use products and packaging purposes, like PP or PS (~30 MPa). Similarly to the tensile strength, the flexural stress at conventional deflection values also dropped with increasing RSS loading, and the rate of reduction was roughly the same. It has to be noted that composites with ≥10 wt% RSS concentration exhibited failure before reaching the point of conventional deflection. Accordingly, in those cases, it is the flexural strength that was reported according to the standard. At high straw concentrations, the intensive agglomeration of particles might also be responsible for the loss in strength, as it deteriorates the effectiveness of load transfer from the matrix to the fiber (Chollakup et al., 2011). Regarding the composites filled with identical amounts of RSS at various sizes it can be observed that the presence of larger particles was
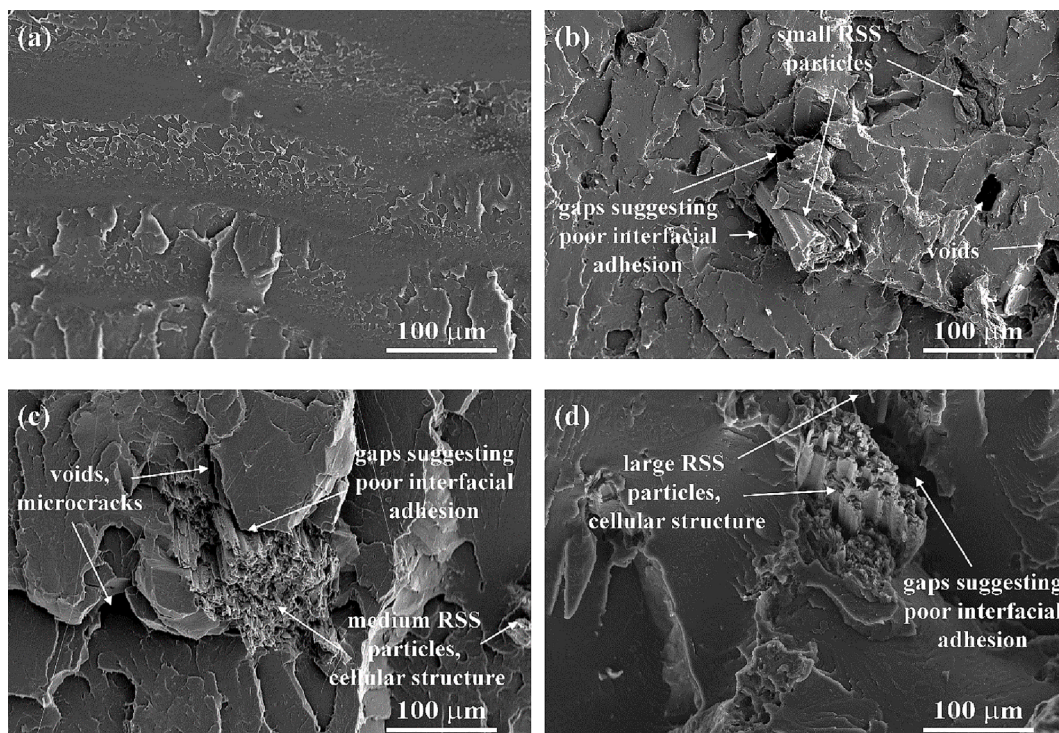
Fig. 3. SEM images of samples PLA (a), PLA_10_S (b), PLA_10_M (c), and PLA_10_L (d).

Table 4
Young's modulus, tensile strength, elongation at break, flexural modulus, and flexural stress at conventional deflection values of PLA-based biocomposites (identical letters in the superscripts are not statistically significantly different at 0.05 according to the Tukey's HSD test; * means flexural strength values are reported instead of flexural stress at conventional deflection since the sample broke before reaching the conventional deflection limit).

Sample	Young's modulus [GPa]	Tensile strength [MPa]	Elongation at break [%]	Flexural modulus [GPa]	Flexural stress at conv. defl. [MPa]
PLA	2.58 ± 0.03[a]	57.3 ± 0.7[a]	4.75 ± 0.86[a]	3.42 ± 0.03[a]	98.8 ± 0.9[a]
PLA_2.5_M	2.63 ± 0.03[a]	52.4 ± 0.7[b]	3.58 ± 0.47[b]	3.53 ± 0.05[b]	96.1 ± 0.7[b]
PLA_5_M	2.76 ± 0.06[b]	50.9 ± 0.6[c]	3.08 ± 0.31[b,c]	3.65 ± 0.03[c]	94.0 ± 1.0[b,c]
PLA_10_M	2.99 ± 0.10[c]	48.3 ± 1.4[d,e]	2.35 ± 0.15[c,d]	4.08 ± 0.02[d]	87.5 ± 1.9[d]*
PLA_20_M	3.42 ± 0.03[d]	46.5 ± 0.2[f]	1.88 ± 0.05[d]	4.41 ± 0.04[e]	79.6 ± 1.6[e]*
PLA_10_S	3.01 ± 0.05[c]	47.5 ± 0.2[d,f]	2.25 ± 0.29[c,d]	3.96 ± 0.05[f]	86.6 ± 2.6[d]*
PLA_10_L	3.17 ± 0.04[e]	49.7 ± 0.4[c,e]	2.12 ± 0.09[d]	4.17 ± 0.04[g]	92.6 ± 1.6[c]*

accompanied by a higher tensile and flexural strength. Accordingly, the sample PLA_10_L exhibited the highest tensile strength out of the various 10 wt% RSS-containing samples (49.7 MPa), while PLA_10_S performed the worst (47.5 MPa). Likewise, the flexural strength of the composites filled with L-sized straw particles (92.6 MPa) was superior compared to the S-, and M−sized straw-containing samples (86.6 and 87.5 MPa, respectively). This effect could be ascribed to the larger aspect ratio of the L-sized straw fibers compared to the M and S as discussed in section 3.1. Larger aspect ratios can better allow stress to be transferred from the matrix to the fibers. Similar observations were made recently in the literature for various polymer matrix/natural filler composite combinations (Zhang et al., 2020; Zhang et al., 2020; Borysiuk et al., 2021).

The Young's modulus of unfilled PLA was 2.58 GPa, which was increased to 2.63, 2.76, 2.99, and 3.42 GPa for the composites containing 2.5 wt%, 5 wt%, 10 wt%, and 20 wt% of M−sized RSS, respectively. These modulus values are much higher than that of PP (~1.3 GPa) and comparable to that of PS (~3.2 GPa). Parallel to the enhancement of Young's modulus, the flexural modulus also exhibited an increment as a function of filler loading, peaking at 4.41 GPa for the PLA_20_M sample, which is relatively ~30% greater than that of neat PLA (3.42 GPa). Generally, the incorporation of agricultural residues into various polymer matrices tends to produce such a boost in stiffness due to the particles acting as rigid fillers within the composite. The sole reason for the modulus values of the composites showing an opposite trend compared to the strength is the fact that the latter is greatly affected by the quality of adhesion between the components, while it does not play a crucial role at low levels of mechanical loads, in which stage Young's modulus is determined.

The elongation at break considerably decreases with increasing RSS content. This reduction can be attributed to the higher degree of brittleness caused by the addition of straw fibers. The incorporation of RSS decreases the chain mobility leading to lower flexibility and making the polymer more rigid. Meanwhile, it is also reasonable to conclude that due to the limited interfacial adhesion, the straw particles may act as stress concentration sites, thereby leading to early failure when the composite is exposed to a critical level of mechanical load. The same explanation can be applied for the samples with high RSS-loading breaking before reaching the conventional deflection limit during the 3-point bending test. In this respect, there were no significant differences between the samples with different straw sizes; all the results were within the deviation range.

Charpy impact strength

The impact strength of neat PLA and its RSS particulates-filled biocomposites with different straw concentrations and straw sizes are shown in Fig. 5a and Fig. 5b, respectively. The average impact strength of unnotched PLA specimens was found to be 15.01 kJ/m², which is
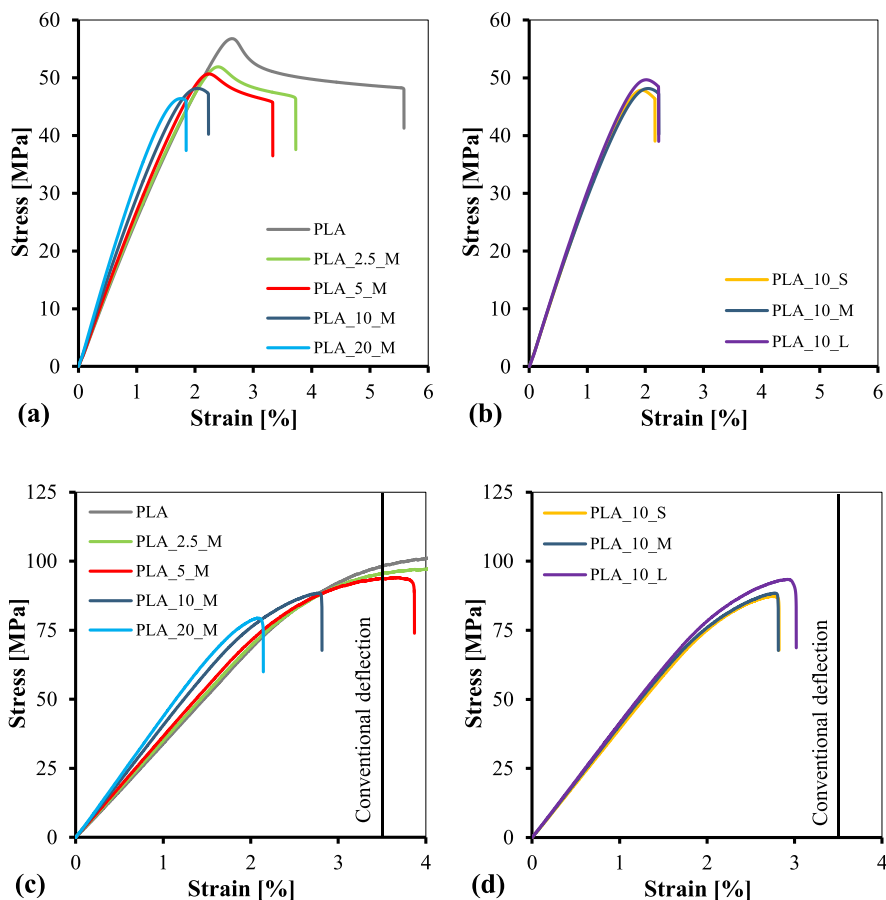
Fig. 4. Characteristic tensile and flexural curves of PLA-based biocomposites with different RSS concentrations (a, b) and RSS sizes (b, d).
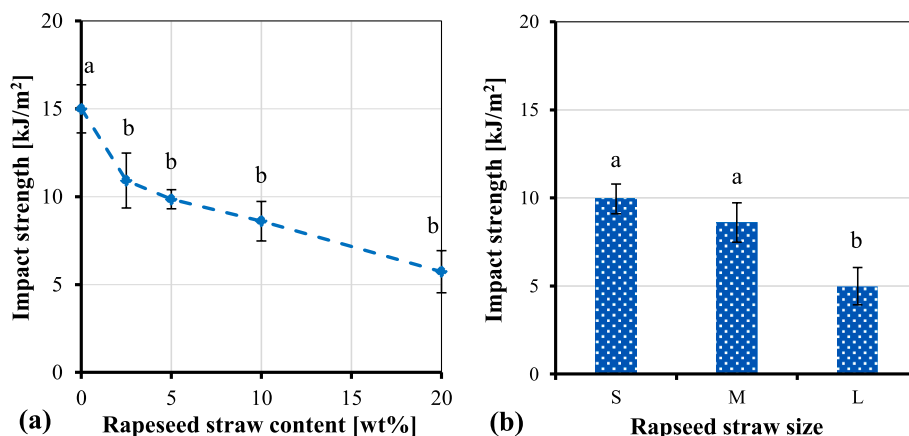

Fig. 5. Charpy impact strength of PLA-based biocomposites with 0–20 wt% RSS of 60–120 mesh (a) and PLA-based biocomposites with different RSS sizes at 10 wt% concentration – S: 120–250 mesh; M: 60–120 mesh; L: 35–60 mesh (identical letters above the markers/bars are not statistically significantly different at 0.05 according to the Tukey's HSD test).

rather close to the values reported in previous studies (Lendvai et al., 2023). Considering the straw fiber concentration, it led to gradually declining toughness. Similar findings were described in the literature for NFRPCs filled with various matrices and fibers (Singh et al., 2023a; Nourbakhsh et al., 2008; Golmakani et al., 2021; Yu et al., 2016). The lignocellulosic particulates in the PLA matrix act as stress concentration points, thereby providing sites for crack initiation and potential composite failure (Nourbakhsh et al., 2010). The impact strength of the PLA/RSS composites bottomed at 5.73 kJ/m^2 for the 20 wt% RSS-containing composite; however, there was no significant difference regardless of the

RSS loading in the whole range of 2.5–20 wt% according to the statistical analysis. The loss in toughness can be ascribed to the rigid characteristics of RSS fibers and to the incomplete wetting of the straw fibers with the PLA resin due to the hydrophilic nature of straw and the hydrophobic nature of PLA, resulting in reduced interfacial bonding and strength with increased filler content. Fig. 5b shows that the particle size of the straw fillers also significantly affects the impact properties of PLA. Among the samples containing 10 wt% straw of various sizes, the sample filled with the smallest S–sized particles exhibited the highest impact resistance, while a deterioration in toughness was observed with

increasing particle size. In terms of toughness, PLA itself behaves rather poorly, thereby, it is obviously no competitor of PP regarding this property, especially when filled with straw fibers. Meanwhile, its impact strength is still comparable to that of PS.

Dynamic mechanical behavior

The results of the DMA measurements are revealed in Fig. 6. The effect of RSS content on the storage modulus of PLA as a function of temperature is depicted in Fig. 6a. In the lower temperature ranges PLA exhibits a glassy state indicated by a considerably high storage modulus, which drastically starts to drop at 55–60 °C due to the glass transition of the material. The initial modulus of over 2.5 GPa falls below 0.005 GPa at this point. This section of the curve, where the modulus is this low is mostly referenced as the first rubbery plateau of PLA in the literature (Cristea et al., 2020). In the range of 90–110 °C a rise can be observed, which occurs as a direct result of cold crystallization, which was enabled by the increased mobility of chain molecules at this elevated temperature. The increased stiffness can be attributed to the confinement effect of crystalline arrays exerted on the diminished amorphous phase. From here on is the second rubbery plateau of the polymer with a roughly constant storage modulus of ~ 0.1 GPa, which lasts until the melting of the crystalline structure (Cristea et al., 2020). Compared to unfilled PLA, the storage modulus of the RSS-filled PLA composites increased in the whole analyzed temperature range. The sample containing 20 wt% straw fibers exhibited the highest storage modulus, followed by the 10 wt%, 5 wt% and 2.5 wt% containing ones, with the last one being almost identical with unfilled PLA, their curves mostly overlapping. These

results are in good agreement with the trends observed in the modulus values during the tensile and flexural tests. Fig. 6b shows the loss factor (*tan δ*) curves of the samples containing different amounts of RSS. The curves show one major peak, corresponding to the glass transition temperature of PLA. Based on the peak maximums, all the samples showed a T_g between 66 and 68 °C with PLA having the highest one, which is in good accord with the DSC results, even though the actual T_g values were slightly higher in this case. This difference is normal, since DMA measurements are typically performed at a specific frequency with a mechanical load being applied and thus the observed transition is the dynamic glass-to-rubber transition process, while during the DSC analysis a calorimetric glass-to-rubber transition temperature is detected. The decrease in glass transition as a function of RSS indicates poor interfacial adhesion between PLA and the straw particles. Fig. 6c and d show the storage modulus and loss factor curves of 10 wt% RSS-filled samples with different straw size. According to the results, with increasing straw particle there is an increased enhancement in the storage modulus, which is again in good agreement with the tensile and flexural tests and represents the better reinforcement efficiency of the larger particles. Meanwhile, the T_g of PLA was not affected by the particle size, the *tan δ* of all samples peaked at the same temperature (~67 °C).

Water absorption

The water absorption behavior of PLA and its RSS-filled composites was investigated by immersing each sample in deionized water at room temperature for 60 days. The data regarding the percentage water
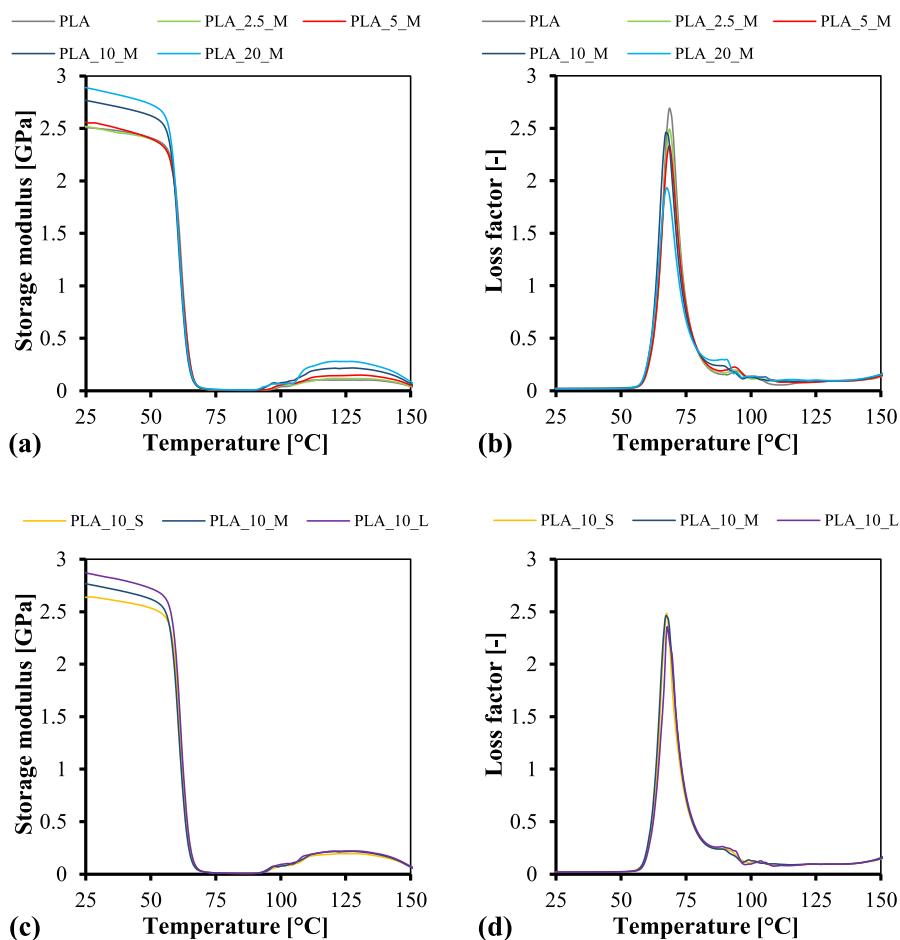

Fig. 6. Storage modulus and loss factor curves of PLA-based biocomposites with 0–20 wt% RSS of 60 120 mesh (a, b) and PLA-based biocomposites with different RSS sizes at 10 wt% concentration (c, d).
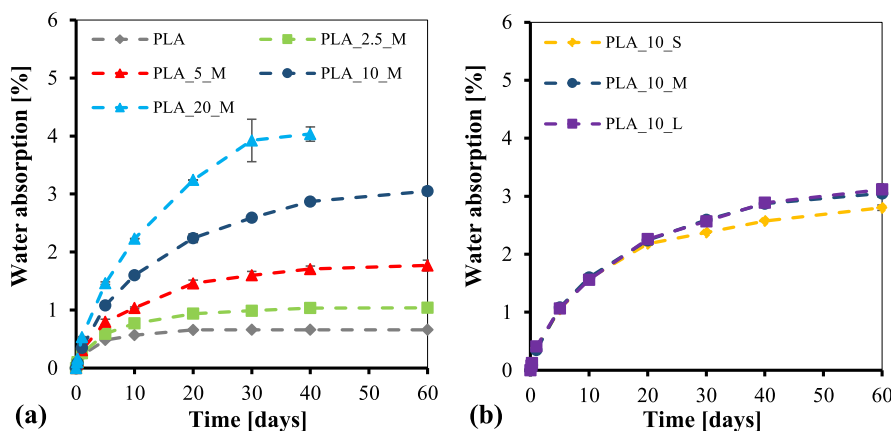
Fig. 7. Water absorption of PLA-based biocomposites with 0–20 wt% RSS of 60–120 mesh (a) and PLA-based biocomposites with different RSS sizes at 10 wt% concentration (b).

uptake, obtained through the gradual monitoring of the samples' weight is shown in Fig. 7. The water absorption behavior of all the prepared samples indicated that the amount of absorbed moisture increases as a function of soaking time. Fig. 7a shows the water absorption of the PLA/RSS samples at different filler loadings. According to the recorded data, the growing amount of straw particles gradually increases the water absorption tendency of the composites, which can be attributed to the hygroscopic nature of the RSS. Besides, capillarity is also suggested to contribute to the penetration of water into the cellular structure of the straw (Mu et al., 2018). As a result, after 60 days, the water uptake of pure PLA (0.7%) increased up to 3%, when 10 wt% M−sized rapeseed straw was incorporated into the polymer. Meanwhile, some specimens of sample PLA_20_M slightly started to disintegrate at this point, with small pieces peeling off from its surface, making it impossible to analyze any further. Nevertheless, its moisture content exceeded 4% even after 40 days, which is considerably higher than any of the other samples'. In the literature, the studies dealing with natural filler loaded PLA composites containing various particles in this amount show similar values of water absorption (~4%), indicating that RSS is a viable option in this regard as well (Ndazi and Karlsson, 2011; Kamaludin et al., 2021; Tee et al., 2017). Regarding the straw particles of different sizes (Fig. 7b), it can be seen that the curves corresponding to the M-sized and L-sized composites were almost entirely overlapping, while the composite with the smallest straw fibers peaked at a somewhat lower moisture content indicating fewer voids, which seems reasonable considering the observations made based on the SEM images.

Cost analysis

The material cost of the prepared samples (€/kg) was calculated based on the cost of the components (PLA and RSS) used to develop the composites and it is presented in Fig. 8. The price of unfilled PLA is the highest (5 €/kg) since it contains the cost of PLA. By incorporating RSS into the polymer, the price of the composites gradually decreased due to the inherently lower cost of waste straw particles (0.25 €/kg). Accordingly, the sample with the highest (20 wt%) RSS content exhibited the lowest material price with 4.05 €/kg. It has to be noted that the costs can depend on many more factors other than raw material costs (additional processing and preparation steps, etc.). Here, however, they are not considered, since any additional costs are dependent on the specific machinery and further field of application.

Conclusion

Interest in using natural fiber reinforced biocomposites instead of synthetic, petrochemical polymer composites has been increasing
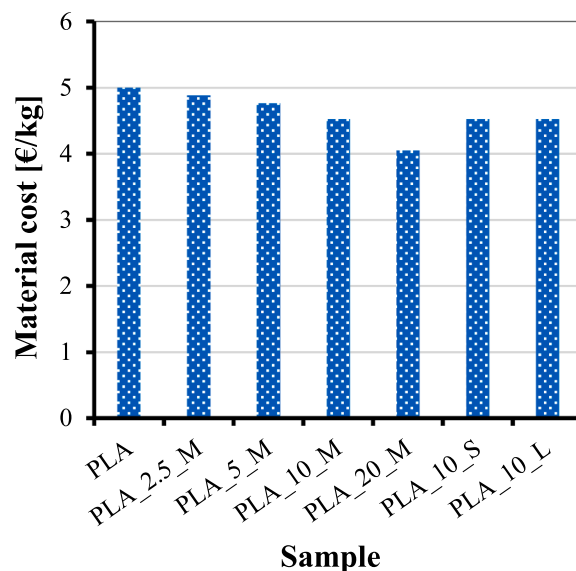

Fig. 8. Calculated material cost of the prepared samples.

steadily to maintain environmental sustainability. From this aspect, utilizing vegetable-based by-products to replace plastics seems to be a viable option to promote a "green" future, since these particles mainly consist of cellulose, lignin, and hemicellulose. Considering these perspectives, PLA/rapeseed straw composites were developed, and their thermal, morphological, mechanical, and physical properties were investigated. RSS was used in different amounts (0, 2.5, 5, 10, 20 wt%) and in different sizes (35–60, 60–120, 120–250 mesh). The DSC analysis showed a decreasing T_g and T_{cc} with increasing RSS content, while the crystallization was facilitated by the straw particles during the heating of composites, indicating that RSS is an effective nucleating agent, especially in the smallest (120–250 mesh) size. Scanning electron microscopic images revealed a limited interfacial adhesion between the matrix and the filler, which also manifested in slightly deteriorating strength properties as seen during the tensile-, flexural- and impact tests. On the other hand, the stiffness of the samples improved by up to ~30% as seen in the enhanced values of Young's modulus and flexural modulus. The water absorption of the biocomposites increased at higher lignocellulose content; however, using smaller particles was an effective way to reduce the water uptake. Overall, rapeseed straw fibers were found to have a prominent potential as additives in biodegradable polymer composites. Even at the maximum analyzed RSS loading, the

mechanical properties were still comparable to those of petrochemical plastics, such as PP or PS that can potentially be replaced with these eco-friendly materials; indeed, in some cases they even exceeded those.

Declaration of Competing Interest

The authors declare that they have no known competing financial interests or personal relationships that could have appeared to influence the work reported in this paper.

Data availability

Data will be made available on request.

References

Amalina, F., Syukor Abd Razak, A., Krishnan, S., Sulaiman, H., Zularisam, A.W., Nasrullah, M., 2022. Advanced techniques in the production of biochar from lignocellulosic biomass and environmental applications. Cleaner Mater. 6, 100137.

Ambrosio-Martín, J., Fabra, M.J., Lopez-Rubio, A., Lagaron, J.M., 2014. An effect of lactic acid oligomers on the barrier properties of polylactide. J. Mater. Sci. 49 (8), 2975–2986.

Beniwal, P., Toor, A.P., 2023. Advancement in tensile properties of polylactic acid composites reinforced with rice straw fibers. Ind. Crop. Prod. 192, 116098.

Bhattacharyya, P., Bisen, J., Bhaduri, D., Priyadarsini, S., Munda, S., Chakraborti, M., Adak, T., Panneerselvam, P., Mukherjee, A.K., Swain, S.L., Dash, P.K., Padhy, S.R., Nayak, A.K., Pathak, H., Kumar, S., Nimbrayan, P., 2021. Turn the wheel from waste to wealth: Economic and environmental gain of sustainable rice straw management practices over field burning in reference to India. Sci. Total Environ. 775, 145896.

Bilal, M., Asgher, M., Iqbal, H.M.N., Hu, H., Zhang, X., 2017. Biotransformation of lignocellulosic materials into value-added products—a review. Int. J. Biol. Macromol. 98, 447–458.

Borysiuk, P., Boruszewski, P., Auriga, R., Danecki, L., Auriga, A., Rybak, K., Nowacka, M., 2021. Influence of a bark-filler on the properties of PLA biocomposites. J. Mater. Sci. 56 (15), 9196–9208.

Chollakup, R., Tantatherdtam, R., Ujjin, S., Sriroth, K., 2011. Pineapple leaf fiber reinforced thermoplastic composites: Effects of fiber length and fiber content on their characteristics. J. Appl. Polym. Sci. 119 (4), 1952–1960.

Cristea, M., Ionita, D., Iftime, M.M., 2020. Dynamic mechanical analysis investigations of PLA-based renewable materials: how are they useful? Materials 13, 5302.

Elsayed, M., Li, W., Abdalla, N.S., Ai, P., Zhang, Y., Abomohra, A.-E.-F., 2022. Innovative approach for rapeseed straw recycling using black solider fly larvae: Towards enhanced energy recovery. Renew. Energy 188, 211–222.

Feng, J.N., Zhang, W.X., Wang, L., He, C.X., 2020. Performance comparison of four kinds of straw/PLA/PBAT wood plastic composites. BioResources 15, 2596–2604.

Gaballah, E.S., Abomohra, A.-F., Xu, C., Elsayed, M., Abdelkader, T.K., Lin, J., Yuan, Q., 2020. Enhancement of biogas production from rape straw using different co-pretreatment techniques and anaerobic co-digestion with cattle manure. Bioresour. Technol. 309, 123311.

Golmakani, M.E., Wiczenbach, T., Malikan, M., Aliakbari, R., Eremeyev, V.A., 2021. Investigation of wood flour size, aspect ratios, and injection molding temperature on mechanical properties of wood flour/polyethylene composites. Materials 14, 3406.

Ji, W., Shen, Z., Wen, Y., 2014. A continuous hydrothermal saccharification approach of rape straw using dilute sulfuric acid. Bioenergy Res. 7 (4), 1392–1401.

Kamaludin, N.H.I., Ismail, H., Rusli, A., Ting, S.S., 2021. Thermal behavior and water absorption kinetics of polylactic acid/chitosan biocomposites. Iran. Polym. J. 30 (2), 135–147.

Lee, S.-Y., Kang, I.-A., Doh, G.-H., Yoon, H.-G., Park, B.-D., Qinglin, W., 2008. Thermal and mechanical properties of wood flour/talc-filled polylactic acid composites: effect of filler content and coupling treatment. J. Thermoplast. Compos. Mater. 21, 209–223.

Lendvai, L., Omastova, M., Patnaik, A., Dogossy, G., Singh, T., 2023. Valorization of waste wood flour and rice husk in poly(lactic acid)-based hybrid biocomposites. J. Polym. Environ. 31 (2), 541–551.

Lendvai, L., Patnaik, A., 2022. The effect of coupling agent on the mechanical properties of injection molded polypropylene/wheat straw composites. Acta Technica Jaurinensis 15, 232–238.

Lendvai, L., Ronkay, F., Wang, G., Zhang, S., Guo, S., Ahlawat, V., Singh, T., 2022. Development and characterization of composites produced from recycled polyethylene terephthalate and waste marble dust. Polym. Compos. 43 (6), 3951–3959.

Mengeloglu, F., Karakus, K., 2008. Thermal degradation, mechanical properties and morphology of wheat straw flour filled recycled thermoplastic composites. Sensors 8, 500–519.

Mishra, S.K., Dahiya, S., Gangil, B., Ranakoti, L., Singh, T., Sharma, S., Boonyasopon, P., Rangappa, S.M., Siengchin, S., 2022. Mechanical, morphological, and tribological characterization of novel walnut shell-reinforced polylactic acid-based biocomposites and prediction based on artificial neural network. Biomass Convers. Biorefin.

Mu, B., Wang, H., Hao, X., Wang, Q., 2018. Morphology, mechanical properties and dimensional stability of biomass particles/high density polyethylene composites: effect of species and composition. Polymers (Basel) 10, 308.

Ndazi, B.S., Karlsson, S., 2011. Characterization of hydrolytic degradation of polylactic acid/rice hulls composites in water at different temperatures. Express Polym. Lett. 5 (2), 119–131.

Nourbakhsh, A., Kokta, B.V., Ashori, A., Jahan-Latibari, A., 2008. Effect of a novel coupling agent, polybutadiene isocyanate, on mechanical properties of wood-fiber polypropylene composites. J. Reinf. Plast. Compos. 27 (16-17), 1679–1687.

Nourbakhsh, A., Karegarfard, A., Ashori, A., Nourbakhsh, A., 2010. Effects of particle size and coupling agent concentration on mechanical properties of particulate-filled polymer composites. J. Thermoplast. Compos. Mater. 23 (2), 169–174.

Nweze Nwogu, C., Nwaiwu, U., Uchechukwu Udo, V., James Nwosu, O., Ezenwa Hart, C., 2022. Effect of date seed granules on the mechanical properties of Glass fibre reinforced epoxy composite. Cleaner Mater. 6, 100160.

Pang, B.o., Zhou, T., Cao, X.-F., Zhao, B.-C., Sun, Z., Liu, X.i., Chen, Y.-Y., Yuan, T.-Q., 2022. Performance and environmental implication assessments of green bio-composite from rice straw and bamboo. J. Clean. Prod. 375, 134037.

Pascoli, D.U., Dichiara, A., Roumeli, E., Gustafson, R., Bura, R., 2022. Lignocellulosic nanomaterials production from wheat straw via peracetic acid pretreatment and their application in plastic composites. Carbohydr. Polym. 295, 119857.

W. Pongputthipat, Y. Ruksakulpiwat, P. Chumsamrong, Development of biodegradable biocomposite films from poly(lactic acid), natural rubber and rice straw. Polym. Bull. 2022.

Qi, Z., Wang, B., Sun, C., Yang, M., Chen, X., Zheng, D., Yao, W., Chen, Y., Cheng, R., Zhang, Y., 2022. Comparison of properties of poly(lactic acid) composites prepared from different components of corn straw fiber. Int. J. Mol. Sci. 23, 6746.

Ranakoti, L., Gangil, B., Mishra, S.K., Singh, T., Sharma, S., Ilyas, R.A., El-Khatib, S., 2022. Critical review on polylactic acid: properties, structure, processing, biocomposites, and nanocomposites. Materials 15, 4312.

Ranakoti, L., Gangil, B., Rajesh, P.K., Singh, T., Sharma, S., Li, C., Ilyas, R.A., Mahmoud, O., 2022. Effect of surface treatment and fiber loading on the physical, mechanical, sliding wear, and morphological characteristics of tasar silk fiber waste-epoxy composites for multifaceted biomedical and engineering applications: fabrication and characterizations. J. Mater. Res. Technol. 19, 2863–2876.

Ronkay, F., Molnar, B., Gere, D., Czigany, T., 2021. Plastic waste from marine environment: Demonstration of possible routes for recycling by different manufacturing technologies. Waste Manag. 119, 101–110.

Singh, T., 2021. Optimum design based on fabricated natural fiber reinforced automotive brake friction composites using hybrid CRITIC-MEW approach. J. Mater. Res. Technol. 14, 81–92.

Singh, T., Aherwar, A., Ranakoti, L., Bhandari, P., Singh, V., Lendvai, L., 2023a. Performance optimization of lignocellulosic fiber-reinforced brake friction composite materials using an integrated CRITIC-CODAS-based decision-making approach. Sustainability 15, 8880.

Singh, T., Fekete, I., Jakab, S.K., Lendvai, L., 2023b. Selection of straw waste reinforced sustainable polymer composite using a multi-criteria decision-making approach. Biomass Convers. Biorefin.

Sohni, S., Norulaini, N.A.N., Hashim, R., Khan, S.B., Fadhullah, W., Mohd Omar, A.K., 2018. Physicochemical characterization of Malaysian crop and agro-industrial biomass residues as renewable energy resources. Ind. Crop. Prod. 111, 642–650.

Tábi, T., Hajba, S., Kovács, J.G., 2016. Effect of crystalline forms (α′ and α) of poly(lactic acid) on its mechanical, thermo-mechanical, heat deflection temperature and creep properties. Eur. Polym. J. 82, 232–243.

Tao, Y., Wang, H., Li, Z., Li, P., Shi, S.Q., 2017. Development and application of wood flour-filled polylactic acid composite filament for 3D printing. Materials 10, 339.

Tee, Y.B., Talib, R.A., Abdan, K., Chin, N.L., Basha, R.K., Yunos, K.F.M., 2017. Effect of aminosilane concentrations on the properties of poly(lactic acid)/kenaf-derived cellulose composites. Polym. Polym. Compos. 25 (1), 63–76.

Tian, S.-Q., Zhao, R.-Y., Chen, Z.-C., 2018. Review of the pretreatment and bioconversion of lignocellulosic biomass from wheat straw materials. Renew. Sustain. Energy Rev. 91, 483–489.

Väisänen, T., Haapala, A., Lappalainen, R., Tomppo, L., 2016. Utilization of agricultural and forest industry waste and residues in natural fiber-polymer composites: A review. Waste Manag. 54, 62–73.

Wang, H., Liu, X., Liu, J., Wu, M., Huang, Y., 2022. Facile dispersion strategy to prepare polylactic acid/reed straw nanofiber composites with enhanced mechanical and thermal properties. Int. J. Biol. Macromol. 221, 278–287.

Wang, D., Xuan, L., Han, G., Wong, A.H.H., Wang, Q., Cheng, W., 2020. Preparation and characterization of foamed wheat straw fiber/polypropylene composites based on modified nano-TiO2 particles. Compos. A Appl. Sci. Manuf. 128, 105674.

Wang, C., Zhang, J., Hu, F., Zhang, S., Lu, J.i., Liu, S., 2020. Bio-pretreatment promote hydrolysis and acidification of oilseed rape straw: Roles of fermentation broth and micro-oxygen. Bioresour. Technol. 308, 123272.

Wen, X., Chen, W., Chen, B., Yang, C., Tu, G., Cheng, T., 2020. Does the prohibition on open burning of straw mitigate air pollution? An empirical study in Jilin Province of China in the post-harvest season. J. Environ. Manage. 264, 110451.

Yaashikaa, P.R., Senthil Kumar, P., Varjani, S., 2022. Valorization of agro-industrial wastes for biorefinery process and circular bioeconomy: a critical review. Bioresour. Technol. 343, 126126.

Yasuniwa, M., Tsubakihara, S., Sugimoto, Y., Nakafuku, C., 2004. Thermal analysis of the double-melting behavior of poly(L-lactic acid). J. Polym. Sci. B 42 (1), 25–32.

Yu, M., Huang, R., He, C., Wu, Q., Zhao, X., 2016. Hybrid composites from wheat straw, inorganic filler, and recycled polypropylene: morphology and mechanical and thermal expansion performance. Int. J. Polymer Sci. 2016, 1–12.

Zeleke, T.S., Yihun, F.A., Ayana, M.T., Kassa, M.T., Alemante, M.F., 2023. Enhancing the Thermo-Mechanical Properties of Thermoplastic Starch Films Using Rice Straw Fibers as Reinforcement. Chemistry Africa.

Zhang, X., Li, S., Xu, C., Li, J., Wang, Z., 2020. Study on the mechanical and thermal properties of poly(lactic acid)/office waste paper fiber composites. J. Appl. Polym. Sci. 137 (45), 49390.

Zhang, J., Tashiro, K., Tsuji, H., Domb, A.J., 2008. Disorder-to-order phase transition and multiple melting behavior of poly(l-lactide) investigated by simultaneous measurements of WAXD and DSC. Macromolecules 41, 1352–1357.

Zhang, X., Wang, Z., Cong, L., Nie, S., Li, J., 2020. Effects of fiber content and size on the mechanical properties of wheat straw/recycled polyethylene composites. J. Polym. Environ. 28 (7), 1833–1840.

Žiganova, M., Ābele, A., Iesalniece, Z., Meri, R.M., 2022. Mercerization of agricultural waste: sweet clover, buckwheat, and rapeseed straws. Fibers 10, 83.